Photochemical ionogenesis in solutions of zinc octaethyl porphyrin

S. G. Ballard and D. C. Mauzerall

Citation: The Journal of Chemical Physics **72**, 933 (1980); doi: 10.1063/1.439211
View online: http://dx.doi.org/10.1063/1.439211
View Table of Contents: http://scitation.aip.org/content/aip/journal/jcp/72/2?ver=pdfcov
Published by the AIP Publishing

Photochemical ionogenesis in solutions of zinc octaethyl porphyrin

S. G. Ballard and D. C. Mauzerall

The Rockefeller University, New York, New York 10021
(Received 26 June 1979; accepted 10 October 1979)

Absolute ion yields and the kinetic parameters of ion formation and decay have been determined by transient conductimetry for two photochemical ionogenic reactions of zinc octaethyl porphyrin in a variety of inert organic solvents. One reaction (T–P) involves electron transfer in the encounter complex of the porphyrin triplet state (T) and ground state (P); it is relatively slow ($k_{TP} \sim 10^8 M^{-1}s^{-1}$, and solvent insensitive). The second (T–T reaction) involves reactive collision between two triplets; it occurs at the encounter limit ($k_{TT} \sim 10^{10} M^{-1}s^{-1}$). Neither rate constant depends on solvent dielectric constant. Reaction yields are very dielectric-dependent, however, and provide unusually straightforward experimental access to the problem of geminate ion-pair decorrelation. A two-parameter model is presented in which the initial photochemically-formed ion pair is created by electron tunneling in a specific spin state at nontrivial separation. The electron transfer radii for the two reactions are determined by completely independent analysis of the kinetic and yield data to be ~21 Å, some 7 Å greater than twice the radius of the porphyrin π-electron system. Following e^- transfer, the solvent-separated components of the geminate pair diffuse in their Coulomb field, undergoing both coherent and incoherent changes in their combined spin state as they do so. They either escape beyond the Coulomb radius to give uncorrelated and conductimetrically active doublet ions, or approach to the critical radius for reverse electron transfer to the ground state (G) and, subject to a spin selection rule, are annihilated. The dominant mechanism of spin interconversion appears to be spin–orbit coupling to the molecular rotations rather than nuclear hyperfine interactions. The coupled diffusion and spin relaxation equations are solved numerically by the method of finite differences; theoretical yields of free ions show good fit to the data over five orders of magnitude. Recombination of the escaped and randomized radicals occurs at the electrostatically accelerated encounter limit and conforms well to the Debye–Smoluchowski equation. Rate constants in excess of 2×10^{11} $M^{-1}s^{-1}$ are observed. A third ionogenic mechanism, direct 2-photon ionization of the porphyrin, is briefly reported. We also briefly characterize the weakly ionogenic quenching reaction of the prophyrin triplet state with molecular oxygen.

I. INTRODUCTION

Electron-transfer reactions between molecules in condensed phases are of interest both as fundamental physical processes and because of their central role in biology. A particularly informative aspect of this subject is photoactivated transfer. Molecular excited states have redox properties very different from the ground states and can participate in rapid electron-transfer reactions during their lifetimes. Such reactions are often invoked as mechanisms of luminescence quenching[1] and are relevant to the primary events in photosynthesis.[2] Photoactivated electron-transfer reactions have a number of advantages for experimental study. Photogeneration of excited-state donor/acceptor species gives, in effect, the most rapid mixing possible with other reactive molecules in solution.

The most direct method of investigating photoactivated electron-transfer reactions under conditions where free ions are produced is conductance measurement. It is very much more sensitive than spectrophotometry or ESR, and is in principle workable into the nanosecond region. Its primary weakness is that it gives little information on the identity of the charged species; this information must be obtained by other methods or otherwise inferred. A compensating advantage is that conductance measurement responds only to ions which are electrostatically uncorrelated, whereas free ions may be indistinguishable by absorbance measurement from bound pairs or charge-transfer complexes. The conductance technique can be applied to study of ionogenic systems in general, even to those which are essentially invisible to optical methods.[3]

To date, transient conductimetry has been rather neglected in the study of photoionization, and especially of photochemical ionogenic reactions in solution. A number of workers have applied it to photostimulated electron ejection from molecules in solid host matrices, from which a great deal of information has been obtained on the phenomena of electron ejection, trapping and migration, and of geminate and bimolecular recombination. The system most extensively studied is tetramethyl-*p*-phenylene diamine (TMPD) in frozen hydrocarbon matrices, authoritatively described by Albrecht and coworkers.[4] Electron ejection from the triplet state of TMPD in fluid solutions was studied by Houser and Jarnagin[5] using a combination of conductance and optical measurements. Kawada and Jarnagin also observed photocurrents produced by the bimolecular reactions of the triplet states of a number of aromatic hydrocarbons in solution.[6] Conductimetry has also been applied to study of ionogenic photodissociation of charge-transfer complexes in solution, primarily by Mataga and coworkers.[7]

Investigation of photoionization gives information not only on the redox properties of excited states and mechanisms of ionization but also provides experimental access to a problem of long standing in chemical physics, namely, the recombination of geminate ion pairs. The literature contains much confusion on this subject in addition to few hard experimental facts. Treatments have often calculated pair escape probabilities in terms

 0021-9606/80/020933-15$01.00

of steady-state gradients and fluxes, analogously with Smoluchowski's treatment of diffusion-controlled reactions in solution. We believe that steady-state models are erroneously applied to the pair problem; their only virtue is mathematical simplicity. A thorough calculation of the rates of escape and geminate recombination has been carried out by Schulten and Schulten[11] for the case of the pyrene–*N*, *N*-dimethylaniline system. Noolandi and Hong[24] have investigated the diffusion equation with Coulomb potential and obtained a formal solution to the problem.

The redox reactions of porphyrin excited states are of especial interest because of their relevance to photosynthesis. In addition, much is known of the quantum chemistry of the porphyrins,[8] making it possible to analyze data at this level. Finally, the excited-state redox reactions of porphyrins, properly chosen, are quantitatively cyclical and are not complicated by extraneous photochemistry such as proton transfers or isomerizations. Electron-transfer photoreactions of porphyrins at phospholipid bilayer/electrolyte solution interfaces have been studied by Hong and Mauzerall[9] and in solution by Carapellucci and Mauzerall.[10] The latter workers reported that the triplet state of zinc uroporphyrin in aqueous electrolyte solutions can be reversibly oxidized by a number of electron acceptors. From their analysis, Carapellucci and Mauzerall concluded that e^- transfer occurs at a distance of 22 ± 2 Å, some 11 Å greater than the sum of the reactant radii.

In the present work both a simpler photochemical system and a more direct experimental approach are used. We measure electrical conductance changes following pulsed laser irradiation of dilute oxygen-free solutions of zinc octaethyl porphyrin in various highly purified inert organic solvents. We employ a sophisticated low-voltage pulsed dc conductance instrument and conditions which are electrochemically nonperturbative to high order. Low-energy optical radiation is used, and is absorbed homogeneously by the solution. This contrast sharply with ionization by pulse radiolysis or γ irradiation, where ions are created inhomogeneously in tracks or spurs, making analysis complex and difficult. Photoconduction is due to the production of electrostatically uncorrelated porphyrin radical ions, the formation of which involves three separate and distinguishable processes. In the photophysical mechanism the triplet state is ionized directly by two-photon excitation, analogously with low-energy two-photon electron ejection from TMPD. The two photochemical processes involve electron transfer in the encounter complex either of two triplet state molecules or a triplet plus ground state singlet. From kinetic and yield data it is independently concluded that in all three processes electron transfer occurs through nontrivial thicknesses of solvent. The spin state of the initial charge-transfer complex is shown to be of primary importance in determining the efficiency of generation of free ions. Yields (but not rates) are also sensitive to small applied magnetic fields. A unified model is presented, in which the solvent-separated components of the charge-transfer state either diffuse apart against an unscreened Coulomb potential or, subject to a spin selection rule, are annihilated by reverse electron transfer at a critical approach distance. We employ time-dependent diffusion equations with spin interconversion between singlet and triplet states of the ion pair, analogously with the approach of Schulten and Schulten.[11] The equations are solved numerically.

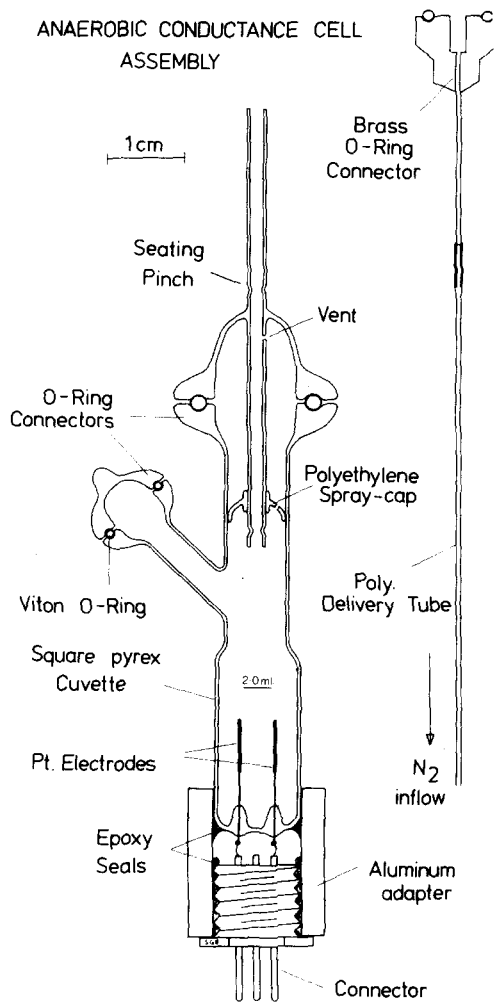

FIG. 1. Anaerobic conductance cell and coaxial purge system.

We confine the present paper to description of methods and observations, with analysis restricted to kinetic interpretation of results and an outline of the theoretical model. A fuller treatment of theory and description of magnetic perturbation measurements is to be given in a later publication.[12]

II. METHODS

The kinetic conductance instrument is described in detail elsewhere.[13] Briefly, it consists of a fast operational current-to-voltage converter, automatic nulling system for compensation and readout of solution background conductance, gated output amplifier, and electronics for bipolar pulse polarization of the electrodes. The detector is used in conjunction with a Pyrex conductance cell (Fig. 1) equipped with a coaxial purge system through which nitrogen gas (Matheson "O_2-free" grade) is flushed to exhaust molecular oxygen from the solution. The N_2 gas is first passed through a copper

coil (~10 ft. length, $\frac{1}{2}$-in.-diam tubing) packed with a chemical oxygen scavenger (BASF R3-11 activated by reduction in hydrogen at 150°C) then presaturated with solvent before delivery to the cell. The limiting lifetime τ_T of the ZnOEP triplet state ($[P] \to 0$) in CH_3CN solution is ~16 ms, probably quite close to the natural lifetime. Residual $[O_2]$ is $\lesssim 10^{-9}$ M (0.1 ppm). The system is sufficiently free of leaks that interrupting the flow for several minutes does not give rise to detectable additional quenching of T. During the purge cycle the gas is bubbled from the bottom of the cell up through the solution; during the measurement the polyethylene delivery tube is lifted just clear of the liquid surface. In order to measure the rate constant and yield of ions produced in the quenching reaction of T and molecular oxygen, dilute solutions (~0.1 μM) of porphyrin were equilibrated with a carrier gas containing a high partial pressure of oxygen (argon + 60 ppm O_2, Ohio).

The electrodes are square flat plates of bright 10-mil platinum sheet 7×7 mm, set 5 mm apart astride the optical axis of the cell. They are pulse polarized at up to ±10 V ($\mathbf{E} \sim 20\,\mathrm{V\,cm^{-1}}$) by application of repetitive bipolar pairs of rectangular voltage pulses of lowest achievable noise figure. The conductance measurement is strictly dc; pulsed bipolar electrode polarization is employed in order to stabilize the solution against electrolysis of the solute and buildup of depletion layers at the electrodes. By adjustment of the times of forward and reverse polarization the solution conductance can be held constant to better than 10^{-10} mho for long periods of time.

Photochemical ion concentration is related to the conductance change following the actinic flash by

$$\Delta K = \sum \lambda_i c_i \frac{A}{1000L}\ \text{mho} \quad \text{(general conductance equation)}$$

$$= \frac{V_s}{V_p}\beta, \quad \text{(instrument transfer function)}$$

where λ_i, c_i are the equivalent conductance and concentration of the ith photogenerated ionic species, L is the electrode spacing, A is the effective area, V_s is the instrument output, β is its transconductance ($\mathrm{A\,V^{-1}}$), and V_p is the cell polarizing voltage.

For generation of uncorrelated univalent ion pairs at concentration $c_\pm$,

$$c_\pm = 1000 V_s / V_p S \lambda_\pm \beta^{-1}\ \text{molar}$$

where S is the cell constant and $\lambda_\pm = \lambda_+ + \lambda_-$. S is determined by calibration of the cell with standard solutions of known equivalent conductance ($Et_4N^+ClO_4^-$ and $\phi_4 B^- Na^+$ in CH_3CN). It is greater than A/L because of conduction in the fringe regions of the cell. There is a small systematic variation in S with solvent dielectric constant, from 2.14 in CH_3CN to 1.98 in diethyl ether (cf. $A/L = 0.98$). S is identical with the ratio of photoconductance signal observed with full-cell illumination to that seen when the actinic light is masked from the fringe region.

λ_i for each photoion is calculated from its friction coefficient (ξ_i). The porphyrin ion radicals are assumed to be equivalent to circular disks of radius $r = 7.8$ Å and thickness $c = 3.4$ Å which obey the Barr–Stokes equation[14] of classical hydrodynamics

$$\xi_i = 6\pi\eta r \left(\frac{1 + 2\eta/\alpha r}{1 + 3\eta/\alpha r}\right) \frac{1}{\frac{9}{16}\pi(1 - 8c/3\pi r)} = 6\pi\eta r_h\ .$$

Stoke's equation for sphere — Barr's disk correction

The $r = 7.8$ Å equivalent hydrodynamic disc is obtained from the flat-face projection of a space-filling model of the porphyrin, scaled to the crystallographic dimensions. It is then reduced to the equivalent hydrodynamic sphere $r_h = 7.0$ Å using the Barr factor (0.898 in this case). α is the coefficient of sliding friction, assumed to be ∞ and η is the cgs kinematic bulk viscosity (Poise). These assumptions are thought to be valid for the motion of large ions in solvents of comparatively small molecules, which then approximate a continuum.[14]

For univalent ions

$$\lambda_i = 10^7 e^2 N/\xi_i\ \mathrm{A\,mol^{-1}}\ (\mathrm{mho\,cm^2\,mol^{-1}}),$$

where e is the electronic (esu) charge and N is Avogadro's number. For $\dot{P}^+$ and $\dot{P}^-$ in CH_3CN at 25°C, $\xi_i = 4.56\times10^{-9}\ \mathrm{g\,s^{-1}}$; $\mathfrak{D}_i (= kT/\xi_i) = 9.03\times10^{-6}\ \mathrm{cm^2\,s^{-1}}$; and $\lambda_i = 30.5\ \mathrm{cm^3\,s^{-1}}$. Equivalent conductances and diffusion constants in other solvents are scaled according to Walden's rule ($\propto \eta^{-1}$).

Because of the variation of ion mobility with solvent viscosity, the instrument sensitivity varies. The instrument sensitivity parameter (Table I, column D) is defined as

$$\omega = V_s/c_i = \beta^{-1} V_p \lambda_i S/1000\ \mathrm{V\,mol^{-1}}$$

$$= 3.98\times10^{-2}\lambda_i\ \mathrm{mV\,nM^{-1}}\ .$$

The kinetic specifications of the instrument are: settling time to 5% = 350 ns; to 0.1% = 500 ns. Detector output noise in 1 MHz B.W. is ~5 mV; single-shot $S/N = 1$ for V_s equivalent to 2×10^{-9} M $\dot{P}^+$, $\dot{P}^-$ at $V_p = 10$ V. By a reasonable amount of coherent averaging (10^3 shots, acquisition time 100 s) 10^{-10} M ions can be detected at 1 μs/digitizer channel (Fabri-Tek FT952). Bandwidth reduction and digitization at 50 μs/channel or slower (FT1052) permits measurement to $c_\pm < 10^{-12}$ M (10^{-5} of background). High photochemical and electrochemical stability is necessary to take advantage of signal averaging. Strict anaerobicity is mandatory. Yield and kinetic data are obtained using a cycle-of-two scheme in which slow baseline drifts are continuously compensated. These are due to the gradual washing down of water and ionic contaminants from the upper regions of the cell assembly by spray which passes the trap disk. Data are read from the instrument computer via an X-Y recorder and is analyzed "by hand." Modeling is performed on a Hewlett–Packard 9825 calculator.

The conductimeter and Ni–Cd battery power supplies are contained in a Faraday cage, single-point grounded. All digitizing and display equipment is powered via an ultraisolation transformer (Topaz 0111T355R). All control signals are transmitted electro-optically: no electrical connection is permissible between laser and signal-handling equipment.

Solvents are prepared by standard procedures.[15]

TABLE I. Columns A–C: physical properties of experimental solvents. Column D: instrument sensitivity parameter, $\omega = 1.05\eta$ nM mV^{-1}. Columns E and F: absolute yield and second-order rate constant of T–P reaction at 25 °C. Columns G and H; absolute yield and second-order rate constant of T–T reaction at 25 °C. Column I: second-order rate constant for P^+, P^- recombination reaction at 25 °C.

Solvent	A $\epsilon^{25\,°C}$	B r_c (Å)	C $\eta^{25\,°C}$ cp.	D ω^{-1}	E ϕ	F k_{TP} ($\times 10^8$)	G ϕ'	H k_{TT} ($\times 10^{10}$)	I k_{+-}
N-Me propionamide	172.2	3.26	5.215	5.50	0.20 ± 0.02	1.4	•••	•••	•••
Dimethyl sulfoxide	46.68	12.0	1.996	2.10	0.27 ± 0.02	4.0	0.233 ± 0.03	(0.5 ± 0.05)	$(5.5 \pm 0.5) \times 10^9$
Acetonitrile	37.50	14.9	0.346	0.36	0.29 ± 0.01	2.0	0.206 ± 0.02	(3.1 ± 0.05)	$(2.0 \pm 0.2) \times 10^{10}$
Propionitrile	27.20	20.6	0.422	0.44	0.33 ± 0.02	2.3	0.134 ± 0.02	(2.5 ± 0.05)	$(3.2 \pm 0.3) \times 10^{10}$
Butyronitrile	20.30	27.6	0.573	0.60	0.36 ± 0.02	2.2	0.072 ± 0.01	(1.9 ± 0.05)	$(3.0 \pm 0.3) \times 10^{10}$
N-Me valeronitrile	15.50	36.2	0.889	0.93	0.37 ± 0.02	2.2	•••	•••	•••
1,2-dichloroethane	10.36	54.1	0.872	0.92	0.083 ± 0.01	2.0	•••	•••	•••
o-dichlorobenzene	9.93	56.4	1.325	1.40	0.105 ± 0.01	2.7	0.019 ± 0.002	(1.2 ± 0.05)	$(2.2 \pm 0.4) \times 10^{10}$
Tetrahydrofuran	7.58	74.0	0.460	0.48	0.042 ± 0.003	1.6	$(1.08 \pm 0.1) \times 10^{-2}$	•••	•••
Ethyl acetate	6.02	93.1	0.426	0.45	0.016 ± 0.002	1.6	$(7.23 \pm 1.0) \times 10^{-3}$	(2.5 ± 0.2)	$(3.6 \pm 0.8) \times 10^{10}$
1-chloronaphthalene	5.04	111.2	2.940	3.10	$(3.97 \pm 0.4) \times 10^{-3}$	2.0	•••	•••	•••
Diethyl ether	4.33	129.5	0.242	0.26	$(1.99 \pm 0.1) \times 10^{-3}$	2.0	$(1.10 \pm 0.1) \times 10^{-3}$	(4.1 ± 0.1)	$(2.9 \pm 0.5) \times 10^{11}$
Anisole	4.33	129.5	0.910	0.96	$(1.40 \pm 0.2) \times 10^{-3}$	2.3	$(1.27 \pm 0.1) \times 10^{-3}$	(1.1 ± 0.2)	$(6.0 \pm 0.5) \times 10^{10}$
Isopropyl ether	3.90	143.7	0.379	0.40	$(1.01 \pm 0.1) \times 10^{-3}$	2.3	•••	•••	•••
n-Butyl ether	3.08	182.0	0.648	0.68	$(1.10 \pm 0.2) \times 10^{-4}$	1.8	•••	•••	•••
n-Pentyl ether	2.77	202.4	1.010	1.06	$(8.60 \pm 2.0) \times 10^{-5}$	1.8	$(1.65 \pm 0.3) \times 10^{-5}$	(1.0 ± 0.4)	$(7.0 \pm 2.0) \times 10^{10}$
Toluene	2.38	235.5	0.552	0.58	$(1.68 \pm 1.0) \times 10^{-5}$	2 ± 1	$(3.80 \pm 1.0) \times 10^{-6}$	(2.0 ± 1.0)	$(1.8 \pm 0.6) \times 10^{11}$
Benzene	2.275	246.4	0.603	0.63	$(0.93 \pm 0.3) \times 10^{-5}$	2 ± 1	•••	•••	•••

First they are chemically dried, fractionally distilled, stored over 3 Å molecular sieves (Linde), then refractionated from sieves directly into the conductance cell. The cell is repeatedly filled then emptied by aspiration until solvent conductance has fallen to its limiting value. Distillations are done in an all-Pyrex apparatus, under dry nitrogen or reduced pressure if necessary. Solvent purity is assayed conductimetrically. The conductance of the solvent has two components. An approximately invariant component $[(0.5\text{–}2) \times 10^{-8}$ mho] is due to ionic impurities (mostly detergent plus lipids) from the glass of the conductance cell; it reaches it full value when the spray from bubbling has "washed" the upper reaches of the cell assembly. The variable component depends on solvent polarity, ranging from $\sim 10^{-9}$ to 10^{-7} mho and is due to H_3O^+ and OH^- (1–100 nM) derived from contaminant trace water. This part of the residual conductance may be abolished entirely by electrolytic drying. In this procedure the cell is continuously polarized at 100 V dc, and the solvent slowly bubbled with dry N_2 gas. Water is electrolyzed and removed as H_2 and O_2. Addition of conductivity water dramatically increases the solvent conductance, but it is quantitatively restored to the invariant level by the above technique.

Note that the electrode polarization voltages are extremely small compared with standard practice. Ion drift velocities are of the order of 100 Åms^{-1}, so that deviations from the thermal velocity distribution and Wien effects are negligible.

Porphyrin is added to dry solvent in the conductance cell in the form of microliter volumes of a 100 μM stock solution made up in dry purified CH_2Cl_2. For acid/base titrations, H_3O^+ and OH^- are introduced in the form of microliter volumes of 10^{-3}M $HClO_4$ and $Et_4N^+OH^-$ in pure CH_3CN. Water titrations similarly employ solutions (50 mM) of conductance-quality H_2O and D_2O in CH_3CN.

The pyridine adduct of ZnOEP is prepared in situ by addition of millimolar pyridine (purified by drying over KOH, followed by double fractional distillation in glass), and identified spectrophotometrically. Absorption spectra were recorded with a Cary-15 spectrophotometer with sample compartment modified to accept the plug-in conductance cell. Pulsed actinic radiation is provided either directly by a nitrogen laser (Molectron UV1000; peak power 1 MW, FWHM 7 ns) at 337.1 nm or via a liquid dye laser (100 kW peak power; FWHM 5 ns) pumped by it. The dye laser is cavity tuned to excite the porphyrin at the peaks of the Soret or visible bands, or in the interband regions. Excitation wavelengths are shown in Fig. 2. Full-cell illumination is employed in all cases. The N_2-laser beam is directed to the Faraday cage by a long-focus concave mirror, then collimated by a confocal quartz biconvex lens. The dye laser beam is projected through a 1 mm aperture mask then a ×25 Galilean telescope. Beam attenuation is done with standard Schott neutral filters (No. NG4-11) calibrated across the working range (337–600 nm) with the Cary-15. Choice of laser, and excitation wavelength, is primarily dictated by the desired fractional conversion (θ) of the porphyrin to the triplet state. The N_2 laser is used to strongly excite the porphyrin ($0.2 > \theta > 10^{-2}$) for studying the T–T reaction and, with attenuation, to verify the yield and kinetic parameters of the T–P reaction following weak excitation ($\theta < 10^{-3}$) in the UV. The bulk of the data on the T–P reaction and the two-photon ionization process is obtained with the LDL, which in addition to providing actinic radiation at many wavelengths also gives a more uniform field (less than ± 5% variation across the 1 in. diameter of the expanded beam). Pulse energy densities are measured with a YSI Model 65 radiometer calibrated against a Scientech Model 36-001 bolometer. The bolometer has internal electrical calibration.

III. RESULTS

This paper is based upon measurements of electrical conductance transients observed in dilute solutions of

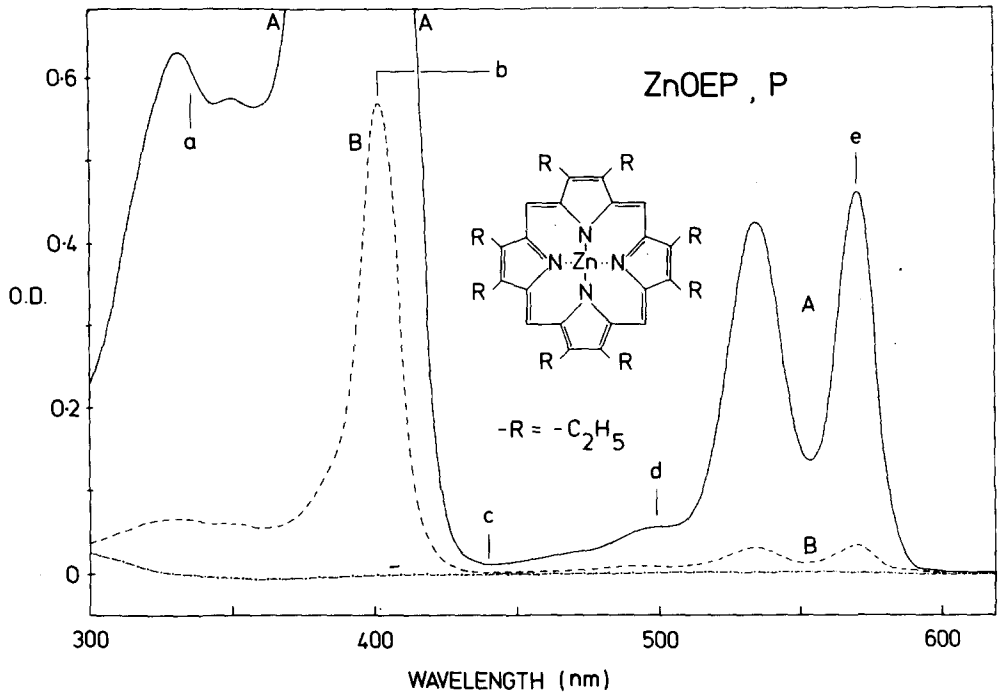

FIG. 2. Zinc octaethyl porphyrin (ZnOEP, P); optical absorption spectrum in CH_3CN. (a) Solid trace; $[P] = 20\ \mu M$, $\epsilon = 5\times10^3$ per 0.1 o.d. (B) Dotted trace; $[P] = 1.5\ \mu M$, $\epsilon = 6.67\times10^4$ per 0.1 o.d. Irradiation parameters: (a) N_2 laser, 337.1 nm, $\epsilon = (3.1\pm0.1)\times10^4$; $\sigma = 1.19$ Å^2. (b) α-NPD LDL, 404 nm, $\epsilon = (3.86\pm0.1)\times10^5$; $\sigma = 14.8$ Å^2. (c) Coumarin 120 LDL, 440 nm, $\epsilon = 810\pm30$; $\sigma = 0.03$ Å^3. (d) Pilot 481 LDL, 496 nm, $\epsilon = (2.75\pm0.2)\times10^3$; $\sigma = 0.106$ Å^2. (e) $R6G$ LDL, 572 nm, $\epsilon = (2.33\pm0.1)\times10^4$; $\sigma = 0.89$ Å^2. $\sigma = 3.84\times10^{-5}\epsilon$ Å^2: ϵ is the molar decadic extinction coefficient, and σ is the optical cross section of P.

zinc octaethyl porphyrin (ZnOEP, P) in a variety of anaerobic organic solvents, following absorption of pulsed actinic radiation. The kinetics of ionization depend on excitation wavelength and intensity but generally ion formation occurs in millisecond or submillisecond times. Complete recombination follows formation, though being second order the kinetics (Fig. 3) depend on initial ion concentration and may extend from a few milliseconds to many seconds. In our experimental limit (hydrocarbon region) there is essentially no conductance relaxation between the flashes, which cannot conveniently be spaced more than 1 s apart. Under such conditions, however, free ions are generated in such small concentrations (subpicomolar/shot) that their accumulation is negligible. Recombination is accurately second order in neutral aprotic solutions only, hence great care must be taken in solvent preparation. Analysis of conductance data is based on the assumption that the photoproducts are the porphyrin ion radicals $\dot{P}^+$ and $\dot{P}^-$. Experimental support of this is given later (Sec. III F).

Three types of ionization behavior may be observed (Secs. III A–III C).

A. $\theta < 10^{-3}$; $\sigma_P \gg \sigma_T$

Weak excitation [fractional conversion to triplet $\theta = \phi_T(1 - e^{-\Psi\sigma_P}) \sim \phi_T\Psi\sigma_P < 10^{-3}$, where ϕ_T is the intersystem crossing yield, ~ 1; Ψ is the time-integrated flux of the actinic flash, photon cm^{-2}; σ_P is the optical cross section of the porphyrin ground state P at the flash wavelength] of O_2-free micromolar solutions of ZnOEP in the Soret band (404 nm) or either of the two visible bands (532 572 nm) or at 337.1 nm on the high-frequency shoulder of the Soret, produces ionization with exponential formation kinetics (Fig. 4) and second-order decays (Fig. 3) which generally are negligibly slow on the time scale of formation. The risetime τ and yield ϕ (defined as moles of each ion produced per einsteins of photons absorbed) are independent of actinic wavelength and energy, provided that $\theta < 10^{-3}$. Yield is calculated from signal amplitude, assuming the conducting species to be $\dot{P}^+$ and $\dot{P}^-$, and triplet state yield to be 0.9.[16] The ion yield from the triplet state is strongly dependent upon the solvent dielectric constant ϵ (Fig. 4, Table I, column E) though the kinetics of formation are not (Fig. 4, Table I, column F). Neither parameter depends at all on solvent viscosity. Variation of $t_{1/2}$ with porphyrin

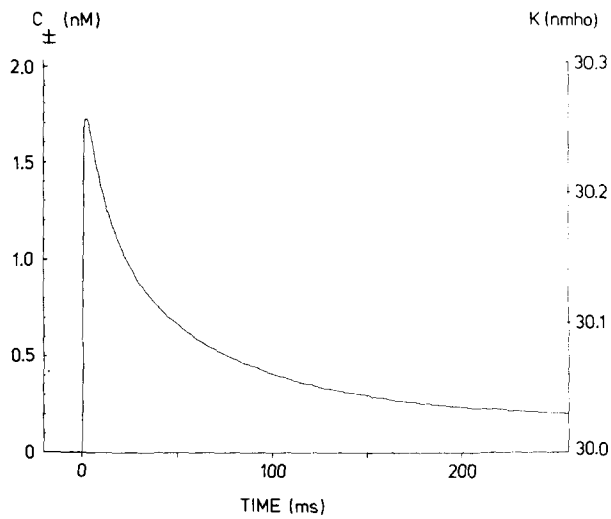

FIG. 3. Photochemical ion formation and recombination in 5 μM ZnOEP solution in dry anaerobic acetonitrile. Trace is average of 16 shots, digitized at 1 ms per point. Static solution conductance: 30×10^{-9} mho, due largely to trace water ($\sim 55\ \mu M$). Initial triplet concentration $T_0 = 5.85$ nM ($\theta = 1.17\times10^{-3}$). $c_{\pm}$ is the concentration of each photogenerated ion ($\equiv [\dot{P}^+] \equiv [\dot{P}^-]$).

concentration compiled from data obtained at several wavelengths is shown in Fig. 5. The kinetics are indicative of a bimolecular reaction between T and P, with P in large excess (pseudo-first-order in P), Sec. IV. k_{PT} is tabulated for the solvents studied in Table I, column F. In all cases it falls within a factor of 2 of $2 \times 10^8 M^{-1} s^{-1}$, about 1% of the encounter limit. Note that extrapolation of the data to zero porphyrin concentration does not pass quite through the origin, indicating that T is quenched to a small extent (~5%) by processes other than reaction with P. The molecularity of this minor loss process cannot be determined from the data. Its insensitivity to the flowrate of the purge gas makes it appear that residual oxygen has a negligible role. Most probably the limiting $t_{1/2}$ for ion formation (~11 ms) represents the natural lifetime of the porphyrin triplet state in solution. As shown in Fig. 4 the formation of ions is complete within a few milliseconds at the standard concentration of 5 μM; the $t_{1/2}$ is in this case about 670 μs. Ion recombination is negligibly slow compared to formation (Fig. 3). The worst case $t_{1/2}$ (corresponding to $[P]_0 = 5$ μM, $\theta = 10^{-3}$, $\phi = 0.5$) is ~30 ms so that the peak conductance change may be used without correction to calculate the ion yield. In high-yield solvents ($\epsilon > 20$), the laser power may be reduced so that $10^{-5} \leq \theta \leq 10^{-4}$, maintaining the $t_{1/2}$ for recombination > 50 ms. The T–P reaction is reversible to better than 1 part in 10^6; recombination of the radicals regenerates the ground state.

B. $0.2 > \theta > 10^{-2}$; $\sigma_P \gg \sigma_T$

Increasing the laser power much beyond $\theta = 10^{-3}$ causes deviation from the exponential formation kinetics of Fig. 4, and ϕ begins to decrease. When $\theta > 10^{-2}$ (achievable only with N_2 laser) the kinetics of ionization are second order (Fig. 7, Sec. IV). Second-order rate

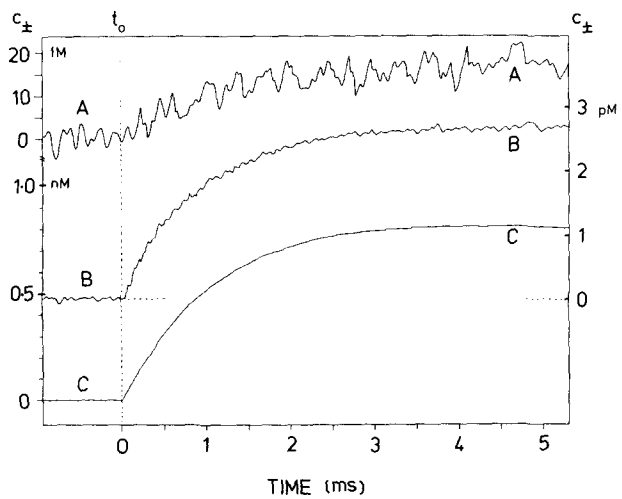

FIG. 4. Kinetics of photochemical ion formation via T–P reaction in three solvents ($\epsilon = 2.275$, 3.90, 37.5). $[P] = 5$ μM Upper trace (A), solvent benzene (top left scale, fM). $N = 131072$. Middle trace (B), solvent isopropyl ether (right scale) pM). $N = 8192$. Lower trace (c), solvent acetonitrile (lower left scale, nM). $N = 16$. In all cases $\theta = 0.5 \times 10^{-3}$; $[T]_0 = 2.5$ nM Digitization at 50 μs/pt.

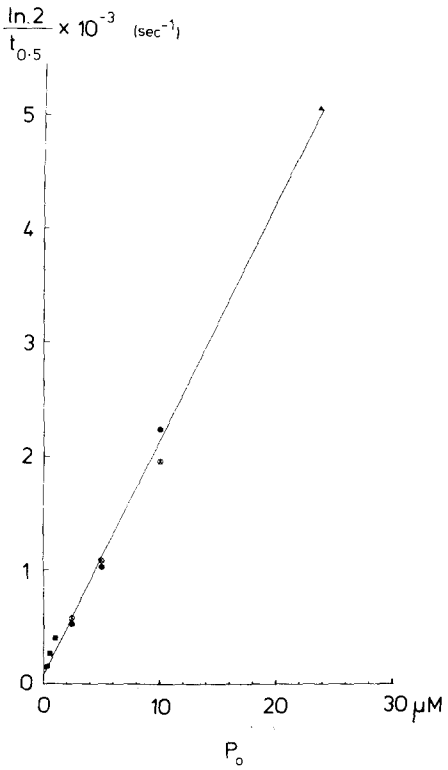

FIG. 5. Ion formation kinetics by T–P reaction; plot of $\ln 2/t_{0.5}$ vs $[P]_0$ for ZnOEP in dry butyronitrile. Key: (▲) Pilot 481 dye laser (496 nm). (⊗) N_2 laser (337.1 nm). (●) Rhodamine 6G dye laser (572 nm). (■) α-NPO dye laser (404 nm). Slope: $k_{TP} = 2.2 \times 10^8$ $1 M^{-1} s^{-1}$. Intercept: ($[P]_0 = 0$) = 65 s^{-1} ($\tau_T = 16$ ms).

constants for this ionogenic process in the solvents investigated are complied in Table I, column H. They show good correlation with η^{-1} (Fig. 11), indicating a diffusion-controlled reaction. Rate constants are independent of solvent dielectric constant ϵ, but yields vary in a manner superficially similar to the T–P reaction. They are systematically lower, however (Table I, column G, Fig. 10). The kinetic behavior strongly suggests that the ionogenic reaction is

$$T + T \xrightarrow{k_{TT}} \dot{P}^+ + \dot{P}^-$$

(Sec. IV). The characteristics of the ion recombination (Sec. IIIE) are identical with the previously described T–P recombination kinetics. Note that k_{TT} is $\sim 100 k_{TP}$, ensuring almost quantitative reaction of T by this mechanism when $\theta \geq 0.05$. All yield data quoted were obtained in the condition $0.1 < \theta < 0.125$. Since the T–T process consumes two triplets for each pair of ions produced, the ion yield is in this case defined as $\phi' = 2x$ moles of each ion produced per Einsteins of photons absorbed. Experimental yields and rate constants in the ten solvents studied are shown in Table I, columns G and H. Yields are plotted versus solvent ϵ and $r_c (= e^2/\epsilon kT)$ in Fig. 10. In high-yield solvents deviations from simple second-order formation kinetics are seen, due to ion recombination on the same time scale as formation. These are corrected by a simple extrapolative method (Sec. IV). In the region $\theta > 0.2$ the second-order T–T kinetics are preceded by an abrupt increase in conduc-

tance, due probably to two-photon electron ejection from the porphyrin via T. There is also degradation of P; the solution changes from pink to an orange color reminiscent of free-base OEP, rather than to the green of the usual photo-oxidation products.

C. $\sigma < 10^{-3}$; $\sigma_T \gg \sigma_P$

Weak irradiation in the region of the trough in the ZnOEP absorption spectrum around 440 nm (Coumarin 120 laser) results in biphasic ionization. At this wavelength the triplet state absorbs very much more strongly than the ground state (molar decadic extinction coefficients are $\sim 10^5$ and 800, respectively, so that the porphyrin is invariably double-hit (Sec. IV). An initial abrupt rise in solution conductance is seen, faster than the detector risetime (350 ns). It is followed by a slow phase, the kinetics of which are identical with the T–P reaction (A). The fraction of the total ionization signal comprised by the abrupt phase is independent of laser power. The absolute yields of both phases depend strongly on solvent dielectric constant. Final (bimolecular) ion recombination is normal, indicating that the ionic products are $\dot{P}^+$ and $\dot{P}^-$.

D. Oxygen quenching

The role of molecular oxygen in the quenching of T is shown in several observations peripheral to our study of porphyrin photoionization. Irradiation of unpurged solutions gives conductance transients with very fast (submicrosecond) risetimes and low yields. Flushing with O_2-free nitrogen establishes ionization kinetics in micromolar porphyrin solutions described in Secs. III A–III C, in which the triplet state is consumed almost exclusively by either the T–P or T–T process, depending on θ, or is directly photoionized.

The extrapolation of Fig. 5 to $[P]_0 = 0$ is thought to indicate the natural lifetime of T rather than the effect of quenching by O_2. The second-order rate constant for the T–O_2 reaction was determined directly from the kinetics of ion formation in the condition

$$k_{TO_2} \cdot [O_2] \gg k_{TP} \cdot [P]_0 + k_{TT} \cdot [T]_0 + k_T \ .$$

This was done by weakly irradiating porphyrin solutions equilibrated with an inert gas (argon) containing 60 ppm O_2 ($[P]_0 = 0.1\ \mu M$, $\theta = 10^{-2}$, $pO_2 = 60$ ppm $\equiv 0.7\ \mu M$ in CH_3CN).

First-order kinetics are observed with encounter-limited rates. The low yield of ions (0.076% in CH_2CN) and scarcity of solubility data for O_2 in obscure organic solvents has inhibited extensive study of the T–O_2 ionization-quenching process for the present. The efficacy of the T–O_2 reaction in quenching photochemical ionization is apparent. Given the low yield of ions, the product is expected to be largely singlet O_2.

E. Ion recombination

Whatever the ionogenic mechanism, the positive conductance transient observed subsequent to the laser flash relaxes precisely to the baseline. The decay kinetics (e.g., Fig. 3) are characteristically second order (Sec. IV) and may extend from milliseconds to many seconds, depending on initial radical concentration. Except in the case of severe irradiation at 337.1 nm, there is no permanent increase in photoconductance.

F. Identification of ions

Despite its tremendous sensitivity, the electrical detection method is essentially nonspecific; the identity of the conducting species must be determined by some other method, or otherwise inferred. Mauzerall and Carapellucci[12] made spectroscopic identification of the ion radicals $\dot{P}^+$ and $\dot{P}^-$ generated by reaction of triplet and ground state of zinc uroporphyrin in aqueous solution, a system similar to the present one. Much of the ionization data presented here is beyond the reach of optical detection ($\Delta C \leq 10^{-9}$M), however. This paper is based on the assumption that the conductance transients are due to formation and decay of the porphyrin ion radicals $\dot{P}^+$ and $\dot{P}^-$. The constancy of ionization behavior in the many solvents employed makes it seem very improbable that they have any role other than as chemically inert dielectric media. Not all solvents behave so. A few were examined and rejected for anomalous ion formation or decay kinetics (dioxane, chloroform, methyl acetate, propylene carbonate), either because they cannot be sufficiently purified or they appear to function as electron acceptors or sources of protons. Protonic solvents such as alcohols were avoided because of their possible proton acceptor–donor reactions with the ion radicals. The conductimetric method is particularly sensitive to such reactions; our study of the photoionization of lumiflavin delineated half a dozen of them previously unsuspected.[3]

Similar reactions can be seen in the present system by adding several-micromolar acids or bases to the solvent. In the carefully purified neutral inert solvents, however, the conductance kinetics are simple both in the formation (pseudo-first-order for $P + T$, second order for $T + T$) and decay phases (second order) and vary little across the very diverse range of solvents studied. The only plausible alternative charge carriers are H_3O^+ and OH^-, formed by proton transfer reactions of the type

$$\dot{P}^+ + 2H_2O \rightarrow \dot{P}(OH) + H_3O^+ \ , \tag{1}$$

$$\dot{P}^- + 2H_2O \rightarrow \dot{P}H + (H_2O)OH^- \ , \tag{2}$$

which involve bimolecular reaction with water present as impurity in the solvent, or

$$\dot{P}^+(H_2O)_2 \rightarrow \dot{P}(OH) + H_3O^+ \ , \tag{3}$$

$$\dot{P}^-(H_2O)_2 \rightarrow \dot{P}H(H_2O) + OH^- \ , \tag{4}$$

involving water ligated to the zinc atom of the porphyrin.

It is desirable to know the extent and rate of these reactions for two reasons:

(a) Measurement of the efficiency of photochemical ionization relies on knowledge of the ion mobilities. H_3O^+ and OH^- have limiting equivalent conductances in CH_3CN of ~ 100 and 130 mho cm^2 mole^{-1}, respectively, compared to 30 mho cm^2 mol^{-1} for $\dot{P}^+$ and $\dot{P}^-$. An error of factor 3.8 in yield arises in the limit of complete conversion. If Reactions (1)–(4) occurred appreciably

faster than the triplet annihilation kinetics (i.e., $\ll 50$ μs for $T-T$ or $\ll 1$ ms for $S-T$) they would not be revealed kinetically. A much slower reaction of $\dot{P}^+$ and $\dot{P}^-$ to produce H_3O^+, OH^- would give biphasic ion formation kinetics, which are never seen. However, all solvents do contain at least micromolar water (0.1 ppm; those of high ϵ may exceed 100 μM), easily sufficient to react with a large fraction of the porphyrin radicals within their lifetime or even the lifetime of the triple state, provided that the rate constants were near the encounter limit.

(b) In high-ϵ solvents where $[H_2O] \sim 100$ μM, pair uncorrelation (defined as separation to the Coulomb radius) occurs in $\leq 10^{-8}$ s; in the low-ϵ region ($[H_2O] < 1$ μM) it takes about 10^{-6} s. In either limit, the concentration of impurity water in the solvent is insufficient by at least two orders of magnitude of react with the nascent ions as they diffuse apart. There is no such restriction, however, on unimolecular formation of H_3O^+ and OH^- from water ligated to the porphyrin, although available data on proton equilibria in hydroxylic solvents makes it appear very unlikely that it would occur in the pair separation time. Thus, the mean lifetime of the HO–H bond in water is about 1 ms; in alcohols it is considerably longer. Nevertheless, to assess the possible involvement of free or bound water, the following experiments were done, using acetonitrile as solvent:

1. Conductance-quality CH_3CN was dehydrated *in situ* by prolonged unipolar cell polarization at 100 V. Water present in the solvent is electrolyzed and removed as H_2 and O_2 by a stream of N_2 gas. During this procedure the solvent conductance was monitored; it falls eventually ($\sim \frac{1}{2}$ h) to about 2×10^{-9} mho, then increases slowly with time to $\sim 2\times10^{-8}$ mho as the upper parts of the cell assembly are washed with spray. We believe that the water content of the solvent is diminished essentially to zero (certainly less than micromolar). Porphyrin photoionization in the extremely anhydrous solvent is virtually indistinguishable from that in standard conductance-grade CH_3CN ($K \sim 30$ n Ω corresponding to ~ 50 μM H_2O).

2. Microliter aliquots of a 55 μM solution of double-distilled water in pure CH_3CN were added to a 2 ml sample of electrolytically dried CH_3CN and the conductance plotted versus $[H_2O]$ added. These data give a measure of the water content of the solvent in subsequent experiments. Incidentally, the K_d of water in CH_3CN may also be estimated from the static conductance titration; $K_d \sim 0.36\times10^{-10}$ mol l^{-1} at 20°C. In the experimental region ($[H_2O] < 20$ μM) the water is 0.06% dissociated; the ion product is $\sim 0.36\times10^{-14}$ mol^2 l^{-2}. The kinetic and yield parameters of the $T-P$ photoionization reaction were measured as a function of $[H_2O]$ over the range 2.2 mM ($\gg [P]_0$) down to the limit of electrolytic drying ($\ll [P]_0$). There is no variation, within experimental error (±5%), either in yield or rate constant.

3. Ligated water was displaced from the porphyrin by addition of a large excess of purified pyridine (~ 1.2 mM) to a 5 μM solution of ZnOEP in dry CH_3CN. Under these conditions the porphyrin is converted quantitatively to the bispyridyl complex. The photoionization is only slightly changed. Yield increases by (20 ± 5)% probably due to small increase in electron transfer radius; formation kinetics are somewhat faster [$k_{PT} = 2.3\times10^8 M^{-1} s^{-1}$ for $P(Py)_2$ vs $2.0\times10^8 M^{-1} s^{-1}$ for $P(H_2O)_2$] and the decay is a little slower [$k_{+-} = 1.48\times10^{10} M^{-1} s^{-1}$ for $P(Py)_2$, vs $1.94\times10^{10} M^{-1} s^{-1}$ for $P(H_2O)_2$]. Slowed recombination is compatible with the more bulky ions.

TABLE II. Compilation of ionogenic photochemical reactions of zinc octaethyl porphyrin (P) and its triplet state (T), (i)–(iv), and bimolecular recombination reaction, (v).

	Reaction	Yield
(i)	$T \xrightarrow{k_T} P$	0
(ii)	$T + P \xrightarrow{k_{TP}} \dot{P}^+ + \dot{P}^-$	ϕ
(iii)	$T + T \xrightarrow{k_{TT}} \dot{P}^+ + \dot{P}^-$	ϕ'
(iv)	$T + O_2 \xrightarrow{k_{TO_2}} \dot{P}^+ + \dot{O}_2^-$	ϕ''
(v)	$\dot{P}^+ + \dot{P}^- \xrightarrow{k_{+-}} 2P$	...

4. The electrolysis method was used to dehydrate a sample of CH_3CN, then a large excess of D_2O (~ 2 mM) was added. The $T-P$ kinetics were unchanged (±5%). If the uncorrelation of the geminate ion pair involved ligated water, a deuterium isotope effect might be expected. None is seen. From these observations we conclude that the species detected conductimetrically are the porphyrin radicals $\dot{P}^+$ and $\dot{P}^-$ and not H_3O^+ and OH^-; neither does water play any role in geminate-pair separation. The only important mechanism of ion destruction is bimolecular recombination, even though the ions may live for many seconds.

IV. KINETIC INTERPRETATION OF DATA

The majority of porphyrins have low internal conversion and fluorescence, and undergo efficient ($\sim 90\%$) intersystem crossing following absorption of light. Formation of ion radicals in dilute O_2-free solutions of porphyrins in organic solvents is observed following excitation with nanosecond laser flashes. The growth of ionization extends over hundreds of microseconds to tens of milliseconds, implying involvement of the long-lived triplet state. The observed kinetics depend upon porphyrin concentration and irradiation parameters as described in Sec. III. They fit accurately the simple kinetic scheme outlined below.

Excitation by a brief optical pulse of wavelength such that $\sigma_P \gg \sigma_T$ generates the photochemically active triplet state in concentration $[T]_0 = [P]_0 \Phi_T [1 - \exp(-\Psi\sigma_P)] = \theta[P]_0$. Recirculation of P via P^* or T is negligible for brief flashes ($\ll \tau_T$) and $\phi_T \geq 0.9$, especially since $\theta \leq 0.15$ in all cases. We interpret the data as follows. After the flash, T decays by four processes (Table II). Process (i) is the unimolecular decay of T and P, with zero yield of ions; Processes (ii)–(iv) are bimolecular reactions of T with P, T and O_2 respectively. All produce measurable ionization, though with very dissimilar efficiencies. Following formation, the porphyrin radical ions recombine bimolecularly (v). The general kinetic

equations for quenching of T and production of ions are complex and unhelpful. Following standard practice we enforce conditions which eliminate one or more of the Processes (i)–(iv) or introduce simplifying assumptions. The anaerobic design of the conductance cell permits removal of O_2 to ~0.1 ppm (10^{-9}M) or less, making (iv) negligible. Hence $dT/dt = -(k_T[T] + k_{TP}[T]\cdot[P] + k_{TT}[T]^2)$.

Further, under all experimental conditions depletion of P by the flash can be effectively ignored in the kinetics. This is self-evident for $\theta < 0.05$. When $\theta > 0.05$, the $k_{TT}[T]^2$ term dominates, because $k_{TT} \sim 10^2 k_{TP}$ (Table I), so that the term dependent on P becomes negligible. The second term $k_{TP}[T]\cdot[P]$ can only be investigated in the pseudo-first-order limit $[P] \gg [T]$. With these approximations, the integrated rate equation for T is

$$[T](t) = [T]_0(Z/[x(e^{Zt} - 1) + Z\,e^{Zt}]) ,$$

where

$$Z = k_T + k_{TP}[P]_0 , \quad x = k_{TT}[T]_0 .$$

By reducing x sufficiently, quenching of T by Process (iv) can be made negligible, so that

$$[T](t) = [T]_0\, e^{-Zt} .$$

This corresponds to the T–P reaction (ii) with triplet loss due to unimolecular decay (i), and is found to be essentially the sole ionogenic mechanism when $\theta \leq 10^{-3}$. In this approximation ionization follows simple exponential kinetics, i.e., $[\dot{P}^+](t) = [\dot{P}^-](t) = \phi[T]_0(1 - e^{-Zt})$. A plot of $t_{1/2}^{-1}$ vs $[P]_0$ is linear ($t_{1/2} = \ln 2/Z$) with slope k_{TP} and intercept k_T (Fig. 5). Numerical values of k_{TP} and k_T in butyronitrile are, respectively, $(2.2 \pm 0.1)\times 10^8 \mathrm{M}^{-1}\mathrm{s}^{-1}$ and $(65 \pm 15)\ \mathrm{s}^{-1}$. k_{TP} is tabulated for all solvents in Table I, column F. k_T is solvent invariant. Since (i) is a "loss" process (yield 0) its presence can be seen in the yield data also. Denoting the true yield of T–P reaction (ii) by ϕ and the experimental yield by $\bar{\phi}$ we see that

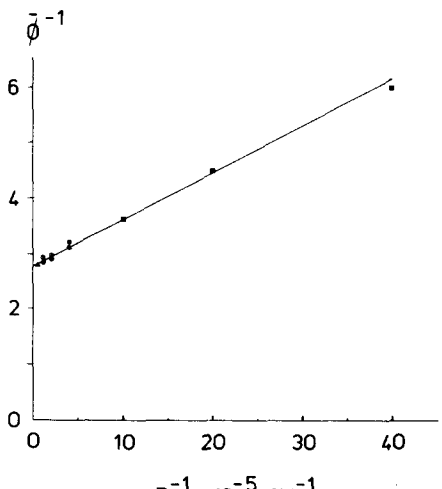

FIG. 6. Experimental yield ($\bar{\phi}$) of T–P reaction; plot of $\bar{\phi}^{-1}$ vs P_0^{-1} for ZnOEP in butyronitrile. Key: See Fig. 5. Intercept: $\phi^{-1} = 2.78$, from which absolute yield $\phi = 0.36$. Slope: $\phi^{-1} k_T/k_{TP} = 0.79 \times 10^{-6}$, from which $k_T = 62.7\ \mathrm{s}^{-1}$.

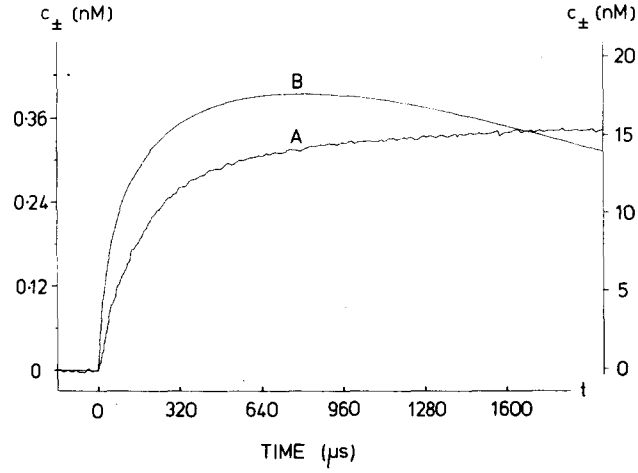

FIG. 7. Kinetics of photochemical ion formation via T–T reaction in 5 μM solutions of ZnOEP. $\theta = 0.12$; $[T]_0 = 0.6$ μM. (A) Solvent anisole; left scale. (B) Solvent butyronitrile; right scale. Both traces average of 16 shots, digitized at 16 μs/pt.

$$\bar{\phi} = \phi\{k_{TP}[P]_0/(k_{TP}[P]_0 + k_T)\} .$$

Figure 6 is a plot of $\bar{\phi}^{-1}$ vs $[P]_0^{-1}$; the intercept is ϕ^{-1} and slope is $\phi^{-1}(k_T/k_{TP})$, from which the natural lifetime of the triplet state $\tau_T = k_T^{-1} = (16.0 \pm 1)\times 10^{-3}$ s is obtained, corresponding to the limiting $t_{1/2}$ for ion formation of ~11 ms. The limiting absolute yield of the T–P reaction is given by the intercept. In butyronitrile it is 0.36 ± 0.02. Note that at $[P]_0 = 5$ μM there is approximately 5% loss of T by unimolecular decay; all T–P yield data in Table I, column E is corrected by this constant fraction. Since the T–P reaction requires that $\theta < 10^{-3}$ it would be difficult to detect even the triplet state decay optically. In solvents of ion yield significantly less than unity, attempts to detect the radicals themselves by ΔOD are probably hopeless.

Observation of the T–T reaction (iii) is much simpler because k_{TT} is close to the encounter limit. This voracious process consumes T virtually quantitatively when $\theta \geq 0.1$. Now $k_{TT}[T] \gg k_{TP}[P]_0 + k_T$ for all but the last few percent of the T decay, so that to a close approximation $[T](t) = [T]_0(k_{TT}[T]_0 t + 1)^{-1}$ and

$$[\dot{P}^+] = [\dot{P}^-] = \frac{[T]_0}{2}\phi'\left(\frac{k_{TT}[T]_0 t}{k_{TT}[T]_0 t + 1}\right) = C_\pm .$$

The data of Fig. 7(A) follow this equation closely. A plot of $C_\pm^{-1}$ vs t^{-1} is linear (Fig. 8), with intercept $\delta = 2/\phi'[T]_0$ and slope $\delta/k_{TT}[T]_0$ from which ϕ' and k_{TT} may be obtained. In solvents of high ϵ, there are small deviations from linearity as $t^{-1} \to 0$ [Fig. 8(B)]. These are due to the distortion of the formation kinetics by bimolecular recombination of the ions, and possibly by some quenching of T by them. The ratio of the $t_{1/2}$'s for the T–T formation process and the $\dot{P}^+$, $\dot{P}^-$ recombination is $\phi'[k_{+-}/k_{TT}]$. Both are second order, so when $t_{1/2}(TT) \ll t_{1/2}(\dot{P}^+\dot{P}^-)$, the recombination produces negligible truncation of the formation kinetics. The two rate constants are approximately equal. The formation kinetics are simple, then, when $\phi' \ll 1$. This is true in all but the highest-ϵ solvents, where some nonlinearity

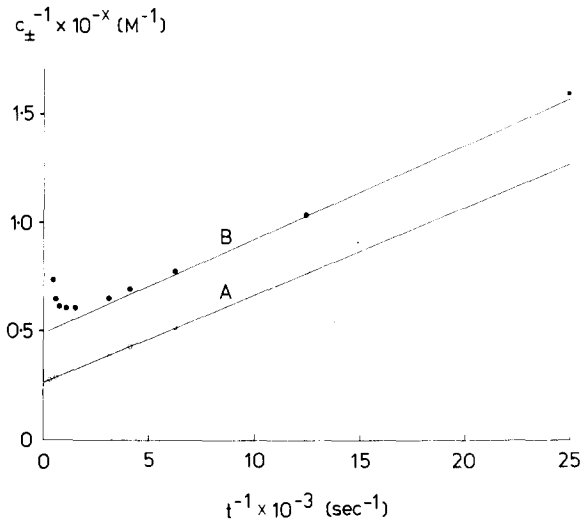

FIG. 8. Ion formation kinetics by $T-T$ reaction; double-reciprocal plot of data in Fig. 7. Trace A: 5 μM ZnOEP in anisole; $X=10$. Intercept: 0.27×10^{10} ($\phi'=1.23\times10^{-3}$). Slope: 4.0×10^{5} ($k_{TT}=1.12\times10^{10}$ l M^{-1} s^{-1}). Trace B: 5 μM ZnOEP in butyronitrile; $X=8$. Intercept: 0.47×10^{8} ($\phi'=0.067$). Slope: 4.2×10^{3} ($k_{TT}=1.87\times10^{10}$ l M^{-1} s^{-1}).

appears in the double-reciprocal plots as $t^{-1}\to 0$. Here the yield data is corrected by extrapolation of the linear ($t\to 0$) region. Recombination data is similarly corrected. Worst-case errors are approximately ±10% but there is little to be gained by more elaborate analyses, which involve fitting the data with at least two second-order rate processes. Reactions (i)–(iii) are thus characterized. The quenching of T and ionogenesis by reaction with O_2 (iv) was briefly studied in a single solvent (CH_3CN) as described in Sec. III D. In the experimental conditions T reacts almost quantitatively with O_2. The $T-P$ reaction ($t_{1/2}\sim 40$ ms), $T-T$ reaction ($t_{1/2}\sim 10$ ms), and unimolecular decay of T ($t_{1/2}\sim 11$ ms) are all negligible. The observed first-order ionization kinetics and very low yields of free ions are interpreted as being due to Process (iv), pseudo-first-order in O_2;

$$[\dot{P}^+]=[\dot{O}_2^-]=\phi''[T]_0\{1-\exp(-k_{TO_2}[O_2]t)\}\,.$$

In CH_3CN, k_{TO_2} is $(3.1\pm0.5)\times10^{10}M^{-1}s^{-1}$ and $\phi''=(7.6\pm2)\times10^{-4}$.

The third distinct type of ionization behavior occurs when $\sigma_T\Psi$ is not negligible, either because σ_T is large or the actinic pulse is very intense. The latter condition is avoided because of irreversible damage to the porphyrin. Ionization within the flash lifetime is thought to involve double hitting of the triplet state, analogously with the biphotonic ionization of TMPD.[4,5] The very high intersystem crossing efficiency makes recirculation of P negligible, so the fluxes of P, T, and T^* will be formally equivalent to two consecutive unimolecular reactions:

$$[T]^*=[P]_0[1+(\sigma_P-\sigma_T)^{-1}(\sigma_T e^{-\Psi\sigma_P}-\sigma_P e^{-\Psi\sigma_T})]\,,$$

which, in the condition of $\sigma_T\gg\sigma_P$, reduces to $[T]^*=[P]_0\times(1-e^{-\Psi\sigma_P})$. This is indentical with $[P]_0-[P]$, meaning that there is a guaranteed second hit of T and quantitative conversion of T to T^*, an electron-ejecting state. Following ejection, the electron may escape and be scavenged, or recombine with $\dot{P}^+$ so as to regenerate T or P, depending on its spin state. The re-formed T is then consumed in the $T-P$ reaction (ii). At 440 nm, $\epsilon_P\sim800$ and $\epsilon_T\sim10^5$ cm^2 mol^{-1}. Further, for the expanded LDL beam at 440 nm, $\Psi\sigma_P\ll1$, so that $[T]^*=[P]_0\Psi\sigma_P$. This is an example of a biphotonic process linear in Ψ. Second-order dependence on Ψ is not seen.

Since the biphotonic ionization is a process distinct from the diffusive bimolecular reactions $T-P$ and $T-T$ its detailed description and analysis is deferred to a separate paper.[17]

The kinetics of bimolecular ion recombination following escape and randomization are simple second order in neutral solvents; double-reciprocal plots ($C_{\pm}^{-1}$ vs t^{-1}) are orthodoxly linear in low-yield solvents and are otherwise trivially correctable by extrapolation. The rate constants k_{+-} for recombination are at the charge-accelerated encounter limit, and conform well to the Debye–Smoluchowski equation (Fig. 9). They are compiled in Table I, column I.

V. MODELING

We interpret the observed conductance transients as being due to the pairwise decorrelation of photochemically-formed ion pairs, followed by random recombination of the escaped ions. The large temporal separation of the decorrelation time and ion mean lifetime (<1 μs vs >10 ms under most experimental conditions) allows a separate treatment of geminate escape and random recombination. We treat the motions of the ions by classical diffusion theory. There is good evidence that this is valid down to the radius of the solvent molecules for the present case of solute radius two to three times that of solvent.[14] The experimental results invite detailed analysis because of their inherent simplicity. Each electron-transfer act and subsequent ion-pair escape or collapse is an isolated event unmarred by collision with any other solute species (P, T, $\dot{P}^+$, $\dot{P}^-$). Previous ex-

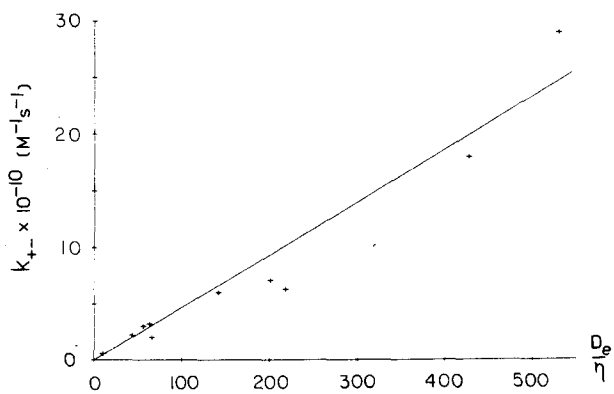

FIG. 9. Ion recombination rate as a function of solvent dielectric constant and viscosity. The second-order rate constants for recombination k_{+-}, (units of 10^{10} l mol^{-1} s^{-1}) are plotted against the Debye factor $D_e\{=r_c/[1-\exp(-r_c/r_m)]\}$ divided by the solvent viscosity (centipoise). A value of 14 Å was used for r_m. Slope of the line equals $NkT/750\,r_h$, where r_h is the equivalent hydrodynamic radius of the ions. Least-squares fit determines r_h to be 7.1±0.4 Å.

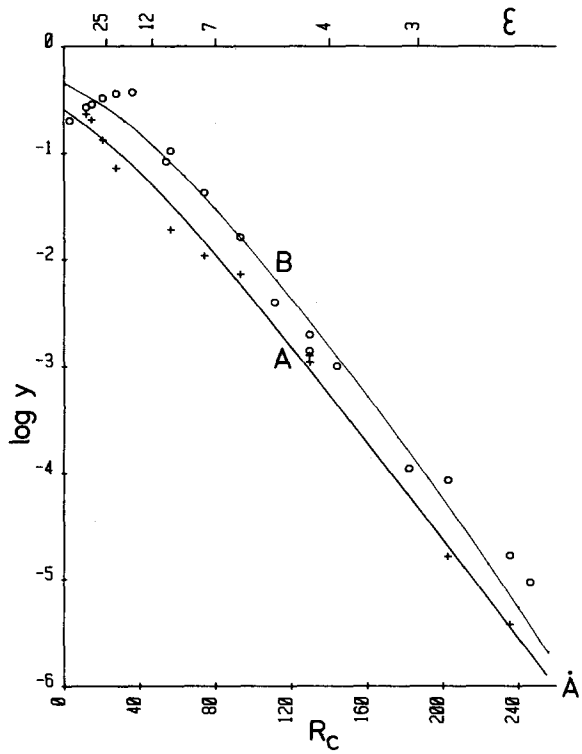

FIG. 10. Ion yield data as a function of solvent dielectric. The logarithms of the ion yields (y) for the T–P reaction (o) and the T–T reaction (+) are plotted vs the Coulomb radius (r_c, bottom linear scale) or dielectric constant (ϵ, top nonlinear scale). Line A is the least-squares fit of the T–T data with Eq. (10). The parameters used are $r_0 = 18.8 \pm 1.1$ Å, $r_m = 14 \pm 3$ Å. Line B is a fit of the T–P data with the model described in Sec. IV. The parameters are $r_0 = 20$ Å, $r_m = 15$ Å, and the spin decorrelation time 0.6 ns.

periments in this field have been conducted under conditions where the concentrations of reactants, products, or even excited states guaranteed collision between these species and the nascent ions. In a solvent of low dielectric constant the ion escape time is many microseconds, and thus concentrations well below 10^{-4}M are required ($< 10^{-6}$M for oppositely charged ions). In the present experiments the ratio of mean interporphyrin distance to the ionic escape radius (i.e., the Coulomb radius r_c) is invariably > 3. This worst-case value pertains to the hydrocarbon solvents. For ion-pair/triplet collisions the corresponding figure is 6 (T–T reaction in benzene), and for collisions between geminate pairs and uncorrelated porphyrin ions it is about 10. The ratios for the T–P reaction are very much larger (> 100 in most solvents). The ability to avoid interaction between the geminate pair and excited states is the major success of the conductance method over conventional flash photolysis.

A. Model

We fitted all the data on ion yields with a very simple model. The reactants T, T or T, P approach one another in a diffusive encounter. At a distance r_0 electron transfer occurs between them. The resulting geminate ions diffuse in their Coulomb field, undergoing both coherent and incoherent changes in their combined spin state as they do so. Of those that come within a distance $r_m (< r_0)$ of each other, rapid reverse electron transfer returns the system to the ground state ($2P$) if the radical pair is in the singlet state. If it is in the triplet state this reaction is forbidden; the back reaction to $T + P$ can however occur. In this model the yield of ions following the electron transfer act is a function of the Coulomb radius of the solvent and of the spin state (and thus spin interconversion rate) of the pair. The influence of spin is shown most dramatically by the greater efficiency of the T–P reaction compared to the thermodynamically far more favorable T–T reaction (Fig. 10).

Four radii enter our discussion, but only two are used as parameters to fit the extensive ion yield and kinetic data. The equivalent hydrodynamic radius r_h was estimated from the molecular dimensions (Sec. II), and is used to scale the conductimetric data to absolute ion yields. It is assumed to be equal for $P, T, \dot{P}^+, \dot{P}^-$ and enters the fitting of k_{+-} and k_{TT} through the combined diffusion constant [Eqs. (5)–(8)]. The reaction radius of $\dot{P}^+$ and $\dot{P}^-$, r_m, is related to the second-order rate constant for random recombination k_{+-} by the Debye–Smoluchowski equation (5) and to the ion yield by Eq. (9). It is only at very low r_c (high dielectric constant) that this parameter significantly affects the data. The electron transfer radius r_0 is related to the second-order rate constant for the T–T reaction, k_{TT}, by the Smoluchowski equation (8) and to the ion yield by Eq. (9). The radii r_0 and r_m are properties of the encounter complexes of the forward and reverse electron-transfer reactions, respectively, and are to be compared with $2r_h$. Each is an average over the complex molecular motions and interactions that characterize reactions in solution. We believe them to be a much better and more fundamental description of the dynamical processes involved than a collection of arbitrary first-order rate constants, which are not applicable to diffusive systems. The fourth radius r_c is the Coulomb radius ($= e^2/\epsilon kT$), and is the measure of the electrostatic interaction in solution. r_c is the scale by which radii derived from ion yields and recombination kinetics are determined. The ion-yield data allows r_0 to be determined within 5%. It is remarkable that knowledge of dielectric constants and ion yields allows determination of a reaction distance to within 1 Å.

B. $\dot{P}^+$–$\dot{P}^-$ recombination

The experimental second-order rate constant k_{+-} for $\dot{P}^+$-$\dot{P}^-$ recombination follows closely the Debye–Smoluchowski equation[18]

$$k_{+-} = \frac{4\pi N D}{1000} \frac{r_c}{1 - \exp(-r_c/r_m)} \ \mathrm{M^{-1}\,s^{-1}} . \tag{5}$$

For most of the solvents the exponential is negligible and the equation reduces to

$$k_{+-} = (4NkT/3000\eta) r_c/r_h , \tag{6}$$

where D (the sum of reactant diffusion constants) has been replaced by the Stokes–Einstein relation.

The data in Fig. 9 is fit with $r_h = 7.1 \pm 0.4$ Å, independently justifying our use of an equivalent hydrody-

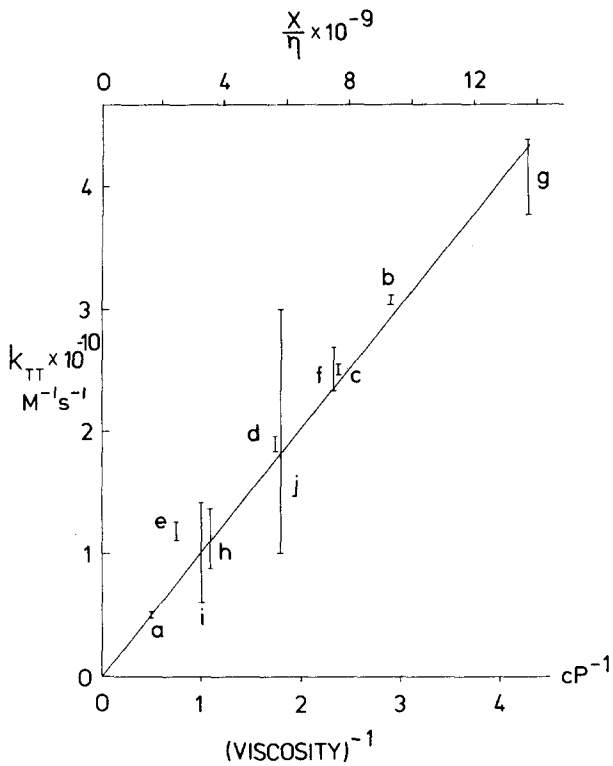

FIG. 11. Correlation between solvent viscosity and experimental second-order rate constant (k_{TT}) for the ZnOEP T–T reaction at 25 °C. Key: (a) DMSO, (b) CH_3CN, (c) CH_3CH_2CN, (d) $CH_3CH_2CH_2CN$, (e) o-$Cl_2C_6H_4$, (f) CH_3COOEt, (g) Et_2O, (h) $=CH_3OC_6H_5$, (i) $Pent_2O$, (j) $CH_3C_6H_5$. $X = NkT/750 = 3.30 \times 10^7$ erg/molecule. Slope: $r_0/r_h = 3.0 \pm 0.17$, from which $r_0 = 21 \pm 1.2$ Å.

namic radius derived from the molecular dimensions (7.0 Å) in calculating the mobilities of the porphyrin radical ions. In solvents of high dielectric constant Eq. (5) reduces to

$$k_{+-} = (4NkT/3000\eta) r_m/r_h , \tag{7}$$

from which r_m can, in principle, be estimated. Our data in this region are very limited, however. They determine r_m to only 15 ± 10 Å. Current experiments with ultrahigh dielectric constant solvents will hopefully refine this value.

C. T–T reaction

Of the two photochemical ionogenic processes we will discuss the T–T reaction first, as it is conceptually the more simple. The reaction is strictly encounter limited, as shown by the linear dependence of the rate constant on the reciprocal of solvent viscosity (Fig. 11). Using the steady-state Smoluchowski equation[19] {the slowness of the reaction renders the transient term $f(t) = [1 + r_0(\pi t D)^{-1/2}]$ very close to unity}

$$k_{TT} = (4\pi ND/1000) r_0 = X(1/\eta) r_0/r_h \ \ M^{-1}s^{-1} , \tag{8}$$

where $X = NkT/750 = 3.30 \times 10^7$ erg/molecule. A plot of k_{TT} vs X/η (Fig. 11) has a slope r_0/r_h. Best fit to the rate data gives $r_0/r_h = 3.0$, i.e., r_0 is 50% larger than twice the hydrodynamic radius of T. Hence $r_0 = 21.0 \pm 1.2$ Å. This is part of our argument that the electron transfer occurs by tunneling (Ballard and Mauzerall[20]). If all of the error in the linear fit of k_{TT} to reciprocal of viscosity is ascribed to ineffective encounters (relative error in zero-constrained least-squares slope $= 0.05$; $r = 0.99$), less than 10% of the encounters are ineffective. This means that the pseudo-first-order rate constant for reaction at r_0 is $\geq 2 \times 10^{10}$ s^{-1}.[21] In other words, if the cage time is 100 ps, electron transfer at the distance r_0 occurs in <10 ps. Thus any tunneling frequency greater than 10^{10} s^{-1} will appear as unity transfer probability. We note that any requirement of specific orientation for reaction will lead to an underestimation of the true r_0. Thus $r_0 = 21$ Å is probably a lower bound. Only the hydrodynamic slowing of reactants approaching closer than twice their radii will cause overestimation of r_0. A layer of "bound" solvent would do the same. However, r_0 is on the outer limit of this effect, and in any case this slowing is essentially the "cage" effect which accounts for the high tunneling probability per encounter in the first place.

Note that k_{TT} is *totally* uncorrelated with other solvent parameters, in particular the Coulomb radius. An important conclusion follows: the solvent polarity has no influence whatsoever on the electron-transfer act. This is just what is predicted by a simple tunneling model of the reaction.[22] The appearance of charge is sudden on the timescale of dielectric orientation relaxation. We assume that the electron tunnels to a site highly polarizable at optical frequencies, and rich with energy levels, viz. the porphyrin acceptor molecule. Note that the usual optical spectra give only a lower limit of the density of states available to the electron because of the particular selection rules for the absorption of electric dipole radiation. Transitions forbidden to single-photon absorption may be allowed to electron transfer (spin 1 vs spin $\frac{1}{2}$). Subsequent interaction with the solvent (low-frequency dipole orientation, etc.) which stabilizes the ions, and the highly entropic diffusion behavior of the geminate pair as it uncorrelates, then contribute to the trapping of the product states. A dependence of the rate of transfer on the optical dielectric constant (i.e., refractive index) is expected.[23]

Let us assume that the T–T reaction produces $\dot{P}^+\dot{P}^-$ in the singlet spin state only. This can be justified as follows: comparison of Figs. 10(A) and 10(B) for the T–T and T–P reaction yields shows that the former must contain $<15\%$ of the latter because of the peak in the T–P yield, or $\leq 5\%$ if the T–T yields at high r_c are to decrease monotonically. The T–P reaction can produce ions which are initially in the triplet state only. A possible mechanism for the T–T reaction is energy transfer to an excited singlet state (as exemplified by the efficient formation of singlet-state oxygen on collision with triplet molecules) and electron transfer which forms the singlet ion pair at r_0.

The problem is to solve the time-dependent diffusion equation with spherical symmetry in the Coulomb field subject to the appropriate boundary conditions

$$\frac{d\mu}{dt} = D\left[\frac{d^2\mu}{dr^2} + \left(\frac{2}{r} + \frac{r_c}{r^2}\right)\frac{d\mu}{dr}\right] , \tag{9}$$

where μ is the probability density of ions separated by distance r at time t. A general solution in closed form is not available (though see Ref. 24), but for the initial condition $\mu_0 = \delta(r_0)$ with boundary conditions $\mu(r_m) = 0$ at all times and yield (y) of ions defined by $\mu(r \to \infty,\ t \to \infty)$, the solution is[25]

$$y = (e^{-r_c/r_0} - e^{-r_c/r_m})/(1 - e^{-r_c/r_m}) \ . \tag{10}$$

It is tempting to try to solve this problem generally by combining simple steady-state solutions of the similar diffusion problem, e.g., the Debye[18] and Eigen[26] equations, as some authors have done. However, the present problem of pair separation involves *strictly transient terms only*, and no steady-state exists. In particular, use of the Eigen equation or first-order kinetics as an "escape rate" cannot be justified. Onsager's equation[27] $y = \exp(-r_c/r_0)$, often quoted in this context, is actually the equilibrium solution and holds only if $r_c \gg r_m$. As $r_c \to 0$ the Onsager equation goes to unity, while Eq. (10) gives $1 - r_m/r_0$.[20] Equation (10) with $r_0 = 18.8 \pm 1.1$ Å and $r_m = 14 \pm 3$ Å is plotted in Fig. 10 (lower curve, A), and fits the data well. We stress that this completely independent analysis confirms the kinetic conclusion that the electron transfer distance r_0 significantly exceeds the sum of the molecular radii. The yield value of r_0 is deliberately minimized, as pointed out above. Any factor causing quenching of T without formation of $\dot{P}^+$ and $\dot{P}^-$ will force a corresponding increase in r_0 to be made. The assumption of a single r_0 to fit all the data is simple parsimony. The intercept of the $T-T$ yield data at $r_c = 0$ determines r_m/r_0, and thus gives estimation of r_m independent of the $\dot{P}^+, \dot{P}^-$ bimolecular recombination kinetics. The yield value is in fact much more precise (14 ± 3 Å). r_0 is determined to within 5% by best fit to all the points. The agreement of the radius values obtained independently from the second-order rate constants k_{TT}, k_{+-} and those given by analysis of the ion yields is strongly supportive of our simple model. Also note that the diffusion constant D does not enter into the solution (10) of Eq. (9), and therefore the ion yields should not depend on solvent viscosity. This is verified by the values of ϕ' for the solvents diethyl ether and anisole at $r_c = 130$ Å, whose viscosities differ by a factor 3.8 but whose ion yields differ by only 15%.

D. *T–P* reaction

If the electron transfer in the $T-P$ reaction occurs by tunneling, the immediate product must be the triplet ion pair. Rephasing of the spin to the singlet state must precede back transfer of the electron to regenerate the ground state $2P$, allowing time for diffusive motion of the ions to occur. Thus the ion yield will be greater than for the energetically far more allowed $T-T$ reaction, and will depend on the triplet to singlet conversion rate.

In our model the diffusive motions of the singlet and triplet ion pairs are coupled in time by the spin interconversion rate. The coupled differential equations are reduced to finite difference equations[29] and then solved numerically. The coupling of the spin and diffusive motions forces an absolute time scale on the modulus of the diffusion equation $D\Delta t/(\Delta r)^2$. Thus, the time for spin relaxation is obtained by scaling and by knowledge of the diffusion constant (Sec. II). Figure 10, curve B shows a fit to the $T-P$ yield data with exponential spin relaxation to the equilibrium $(\dot{P}^+\dot{P}^-)^S : 3(\dot{P}^+\dot{P}^-)^T$ mixture with $\tau = 0.6$ ns, and similar values of r_0 (20 Å) and r_m (15 Å) to the $T-T$ reaction. Brocklehurst[28] showed that rapid dephasing of the spins in such ion-pair states can occur by nuclear hyperfine interactions. Although the timescale for spin mixing is approximately correctly predicted from ESR data on the porphyrin cation and anion radicals, other evidence based on the effect of magnetic fields[12] and solvent viscosity variation supports our view that in the present case the dominant factor in spin dephasing is spin-orbit coupling with molecular rotations. For example, the hyperfine mixing mechanism predicts a threefold decrease in yield at $r_c = 130$ Å for a 3.8-fold increase in viscosity, but only a 30% decrease is observed. The spin–orbit–rotation mechanism predicts no effect to first approximation. The slowed diffusion towards escape at higher viscosity is countered by a corresponding decrease of the spin relaxation rate via rotational diffusion. Hence the differential relaxation per diffusive step is approximately constant, and the yield is independent of viscosity. Note that the fast relaxation time (0.6 ns) required to fit the data is very close to the estimated rotational relaxation time of the porphyrin [Debye $\tau_r = 4\pi\eta a^3/kT = 0.7$ ns in C_6H_6; experimental out-of-plane relaxation time for octaphenyl porphyrazine = 0.3 ns in C_6H_6 (Ref. 30)]. These points will be discussed further elsewhere.[12] If the spin-relaxation rate increases with dielectric constant in very polar solvents the decrease in yield at low r_c (Fig. 10) is also explained.

A weakness of this simple mechanism for the $T-P$ reaction is that the invariance of the second-order rate constant at about 1% of the encounter limit requires a separate explanation. Theoretical calculations give indication of several low-lying triplet states in highly symmetrical porphyrins.[31] Thermal population of a reactive triplet state T' about 0.1 eV higher than the lowest (unreactive) triplet level would account for the solvent-insensitive rate constant and the fact that it is 100-fold below the encounter limit. Reverse electron transfer to the lower triplet state would be energetically favorable and so contribute to ineffective encounters of $P + T$. During the lifetime of the ion-pair dephasing of the electron spin forms $[\dot{P}^+\dot{P}^-]^S$, which collapses to $2P$ at r_m or undergoes escape to form free ions. Its escape probability will be given by Eq. (8), but with the origin of the singlet pair distributed between r_m and r_0; radical pairs separating in the triplet state are assumed to back transfer to $T + P$ at r_0. Assuming only singlet pairs escape as ions, the yield data can be fitted with the same r_m as before (15 Å) but with a somewhat larger value of r_0 (21 Å). The curve is nearly superposable on Fig. 10, curve B. In this extreme case the triplet to singlet decorrelation time will enter only as a determinant of the fraction of effective collisions of P and T'. This time could range from very fast (< 0.1 ns) up to about 1 μs if the ineffective collisions are caused purely by the spin decorrelation time (i.e., $T = T'$). A more

realistic model will allow both $[\dot{P}^+\dot{P}^-]^T$ and $[\dot{P}^+\dot{P}^-]^S$ to escape. If the majority of the escaped ions are singlets this argument predicts weak dependence of yield on viscosity and magnetic field, as is observed. Further analysis is deferred to the following paper.[12]

VI. THERMODYNAMICS

Most discussions of photoinduced electron-transfer reactions compare the energy levels of the ground and excited states of the molecules with the redox potentials of the corresponding oxidized and reduced species.[32] A term involving the Born charging energy is often added as a solvent effect. This term is crude, but agreement is obtained by adjusting the "radius." The relevant data for ZnOEP are: singlet state enthalpy 2.16 eV; triplet state, 1.79 eV (obtained from the peak of emission spectra, having only slight dependence on solvents); $ZnOEP^+ + e^-$, $E_0 = 0.63$ V [polarographic vs sat. Calomel (SC), butyronitrile[33]], +0.53 V (potentiometric vs SC, methanol,[34]); $ZnOEP + e^-$, $E_0 = -1.62$ V (polarographic vs SC, dimethyl sulfoxide[33]). Thus the triplet state would appear to be 0.4 ± 0.1 V below the energy of the anion plus cation in a polar solvent.[36] However, the numbers themselves are weak. The O–O transitions are unknown and approximated by peak emissions. The narrow bands of the porphyrins (< 0.05 eV) do minimize this error. The redox potentials in organic solvents are subject to unknown junction potentials (~0.1 V) to the reference electrode.[35] Almost all organic redox potentials are determined by polarography, not by potentiometry. Again, the porphyrins are an exception.[34] Cyclic voltammetry allows the establishment of questionable criteria for the reversibility of the polarographic measurements.[37] However, almost all one-electron organic redox reactions are irreversible. Thus, these measurements of necessity contain unknown kinetic parameters in addition to the thermodynamic reversible redox potential. It is not surprising that these "potentials" have been found to correlate well with the rate of electron-transfer reactions (see e.g., Ref. 38). From our view the contributions to the irreversibility (tunneling, relaxation, proton transfers, rapid multistep chemical reactions) are the same for two molecules and for the molecule-platimum electron exchange. Finally, and not least, the true thermodynamic redox potentials are a free energy and contain a significant entropic contribution from both internal and external effects.[39] This can be measured: $\Delta S = \partial E_0/\partial T$. This valuable measurement has been sadly neglected, especially in organic systems. The entropic contribution can be overwhelming: e.g., Fe $(H_2O)_6^{3+ \text{ to } 2+}$ has $E_0 = 0.77$ V, $\Delta H_0 = -0.43$ V/mol, $T\Delta S_0 = +0.33$ eV/mol,[40] compared to Fe $(\text{phenanthroline})_3^{3+ \text{ to } 2+}$, $E_0 = 1.14$ V, $\Delta H_0 = -1.41$ eV/mol, $T\Delta S_0 = -0.27$ eV/mol.[41] The usual application of redox potentials results in an *error* of 0.6 V: $\Delta E_0 = 0.37$ V, $\Delta H_0 = -1.0$ eV/mol! Any attempt trivially to relate electrochemical redox potentials to spectroscopic energy levels is doomed to failure.

Aside from these correctable difficulties, the "thermodynamic" approach implies that the electron transfer is an equilibrium or activated-state process. This is very unlikely to be so for encounter-limited reactions. In this case the probability of electron tunneling increases exponentially with decreasing distance between the reactants. This probability is modulated by rotational orientation and by solvent interactions during the diffusive movements, but the integrated probability rises steeply to unity at some distance, which we have labeled r_0. The reverse electron transfer to the previous excited state simply leads to an ineffective collision. The reverse transfer to the ground state requires pairing of electron spins and a closer approach, to r_m ($< r_0$). The reasons for this smaller reaction radius include less orbital overlap for ground compared to excited states (greater barrier height) and a smaller density of states.[22] The ions are able to escape by purely stochastic motion, with probability given by Eq. (10). The driving force for this escape is simply the molar entropy of mixing, and tends to a logarithmic infinity for infinitely dilute solutions. The time scale for the development of this entropic flow is given by the diffusion equation (9). The delay caused by electron spin decorrelation allows the T–P reaction greater access to this source of entropy. For the very dilute solutions employed in the present experiments $T\Delta S$ can amount to several tenths of a volt on the electrochemical scale. Our view is that these particular electron transfer processes are essentially irreversible and can only be described by including a flow of entropy: the diffusive molecular motions, the relaxation processes in the electron spins and in both molecule and solvent following electron transfer. In many other organic systems electron transfer is followed by rapid proton transfers. In most systems rapid and complex chemistry drives the provess even further from the initial state. Thus, the present interpretation of the decrease of ion yield with decreasing dielectric constant differs drastically from the "equilibrium" view. It is not necessarily that electron transfer cannot take place, but that the ions have decreasing probability of escape. The process is highly dynamic and rich in mechanistic detail. It is just these details that are most necessary to explain the exceptionally high efficiencies of the electron transfer reactions of porphyrins. This in turn is a step closer to a basic understanding of the similar processes in photosynthesis.

ACKNOWLEDGMENTS

We thank Professor J.-H. Fuhrhop for his generous gift of the porphyrin. This research was supported by the National Science Foundation, Grant Nos. CHE-7725152 and PCM74-11749 and by the Rockefeller University.

[1] H. Knibbe, K. Röllig, F. P. Schäfer, and A. Weller, J. Chem. Phys. 47, 1184 (1967); N. Mataga, T. Okada, and N. Yamomoto, Chem. Phys. Lett. 1, 119 (1967); K. H. Grellmann, A. R. Watkins, and A. Weller, J. Phys. Chem. 76, 469 (1972); 76, 3132 (1972).
[2] R. E. Blankenship and W. W. Parson, Ann. Rev. Biochem. 47, 635 (1978).
[3] S. G. Ballard, D. C. Mauzerall, and G. Tollin, J. Phys. Chem. 80, 341 (1976).
[4] H. S. Piloff and A. C. Albrecht, J. Chem. Phys. 49, 4891 (1968); K. D. Cadogan and A. C. Albrecht, *ibid.* 51, 2710

(1969).
[5]N. Houser and R. C. Jarnagin, J. Chem. Phys. **52**, 1069 (1970); S. S. Takeda, N. Houser, and R. C. Jarnagin, *ibid.* **54**, 3195 (1971).
[6]A. Kawada and R. C. Jarnagin, J. Chem. Phys. **44**, 1919 (1966).
[7]H. Masuhara, M. Shimada, N. Tsujino, and N. Mataga, Bull. Chem. Soc. Jpn. **44**, 2310 (1971); Y. Taniguchi and N. Mataga, Chem. Phys. Lett. **13**, 596 (1972); Y. Taniguchi, Y. Nishina, and N. Mataga, Bull. Chem. Soc. Jpn. **45**, 764 (1972).
[8]M. Gouterman, in *The Porphyrins*, edited by D. Dolphin (Academic, New York, 1978), Vol. III, p. 1.
[9]F. T. Hong and D. C. Mauzerall, J. Electrochem. Soc. **123**, 1317 (1976).
[10]P. Carapellucci and D. C. Mauzerall, N. Y. Acad. Sci. **244**, 238 (1975).
[11]Z. Schulten and K. Schulten, J. Chem. Phys. **66**, 4676 (1977); H.-J. Werner, Z. Schulten, and K. Schulten, J. Chem. Phys. **67**, 646 (1977).
[12]S. G. Ballard, J. Geronimo, and D. C. Mauzerall (unpublished).
[13]S. G. Ballard, Rev. Sci. Instrum. **47**, 1157 (1976).
[14]A. H. Alwatter, M. D. Lumb, and J. B. Birks, in *Organic Molecular Photophysics*, edited by J. B. Birks (Wiley, London, 1973), Chap. 8, p. 403.
[15]J. A. Riddick and W. B. Bunger, *Organic Solvents, Techniques in Chemistry Series* (Wiley-Interscience, New York, 1970), Vol. II.
[16]A. T. Gradyushko and M. P. Tsvirko, Opt. Spectrosc. **27**, 91 (1971); G. P. Gurinovich and B. M. Jagarov, in *Luminescence of Crystals, Molecules and Solutions*, edited by F. Williams (Plenum, New York, 1973), p. 196.
[17]S. G. Ballard and D. C. Mauzerall (unpublished).
[18]P. Debye, J. Electrochem. Soc. **82**, 265 (1942).
[19]M. von Smoluchowski, Z. Phys. Chem. **92**, 129 (1917).
[20]S. G. Ballard and D. C. Mauzerall, in *Tunneling in Biological Systems*, edited by B. Chance *et al.* (Academic, New York, 1979), p. 581.
[21]R. M. Noyes, Prog. Reaction Kinet. **1**, 129 (1961).
[22]D. C. Mauzerall, in "Chlorophyll-Protein Reaction Centers and Photosynthetic Membranes," Brookhaven Symposia in Biology, No. 28, 1976 (unpublished), p. 64; D. C. Mauzerall, in Ref. 10, Vol. V, p. 29.
[23]A small and uncertain decrease of k_{TT} with refractive index is observed, but we believe that this is simply because the more viscous solvents happen to be more polarizable. Over a narrow range of any variable, such as in the homologous series of four nitriles, one can observe excellent and, we believe, quite spurious correlations. The importance of varying the solvent property over a significant cange cannot be overstressed.
[24]J. Noolandi and K. M. Hong, J. Chem. Phys. **68**, 5163, 5172 (1978).
[25]L. Monchick, J. Chem. Phys. **24**, 381 (1956).
[26]M. Eigen, Z. Phys. Chem. N. F. **1**, 176 (1954).
[27]L. Onsager, J. Chem. Phys. **2**, 599 (1934).
[28]B. Brocklehurst, Chem. Phys. Lett. **28**, 357 (1974).
[29]H. S. Carslaw and J. C. Jaeger, *Conduction of Heat in Solids*, 2nd ed. (Oxford U. P., Oxford, 1959), p. 466; J. Crank, *The Mathematics of Diffusion*, 2nd ed. (Oxford U. P., Oxford, 1973), p. 137.
[30]D. A. Pitt and C. P. Smyth, J. Phys. Chem. **63**, 582 (1959).
[31]J. D. Petke, G. M. Maggiora, L. L. Shipman, and R. E. Christoffersen, J. Mol. Spectrosc. **71**, 64 (1978).
[32]D. Rehm and A. Weller, Ber. Bunsenges. Phys. Chem. **73**, 834 (1969).
[33]J.-H. Fuhrhop, K. M. Kadish, and D. G. Davis, J. Am. Chem. Soc. **95**, 5140 (1973).
[34]J.-H. Fuhrhop and D. C. Mauzerall, J. Am. Chem. Soc. **91**, 4174 (1969).
[35]R. H. Felton, in Ref. 10, Vol. V, p. 56.
[36]The observed rate constant k_{TP} is 1% of the encounter-limited rate and thus allows only ~0.1 eV of activation energy of the process $P+T \rightarrow P^+ + P^-$ in order to reach the encounter limit. However, as is pointed out in Sec. IV, a tunneling frequency of 10^{10} s^{-1} or greater will be seen as unit transfer probability per encounter. The absolute maximum tunneling frequency could be as high as 10^{14} s^{-1} at r_0 if there were no limitation due to orientation requirements, low density of states, etc. This would allow a additional 0.2 eV of activation energy to be present and still give encounter-limited rates. Now the triplet state would be within reach of the "redox" levels. We believe so large a tunneling rate to be quite unrealistic.
[37]D. G. Davis, in Ref. 10, Vol. V, p. 127.
[38]G. R. Seeley, Photochem. Photobiol. **27**, 638 (1978).
[39]R. W. Gurney, *Ionic Processes in Solution* (McGraw-Hill, New York, 1953).
[40]R. E. Connick and W. H. McVey, J. Am. Chem. Soc. **73**, 1798 (1951); G. I. H. Hanania, D. H. Irvine, W. A. Eaton, and P. George, J. Phys. Chem. **71**, 2022 (1967).
[41]P. George, G. I. H. Hanania, and D. H. Irvine, J. Chem. Soc. 2548 (1959).